Proceedings of IMEC2000:
2000 ASME International Mechanical Engineering Congress and Exposition
November 5-10, 2000, Orlando, Florida

A SELF-CONSISTENT TRANSIENT PAINT SIMULATION

Ronald H. Miller
Scientific Research Laboratory
Ford Motor Company
Dearborn, Michigan 48121
Email: rmille47@ford.com

Gary S. Strumolo
Scientific Research Laboratory
Ford Motor Company
Dearborn, Michigan 48121
Email: gstrumol@ford.com

Jake Braslaw
Scientific Research Laboratory
Ford Motor Company
Dearborn, Michigan 48121
Email: jbraslaw@ford.com

ABSTRACT

Optimizing the painting process involves understanding the many nonlinear dynamics that effect paint transfer efficiency (PTE) such as bell applicator design (bell cup and shaping air ring), operating conditions (shaping air flow rate, paint flow rate, electric potential, downdraft, and bell rotation speed), target location, and paint type. PTE optimization results in less experimental testing and improved paint quality. We have modified a numerical simulation to include self-consistent momentum coupling between a continuum and discrete mass particles, as well as the inclusion of a self-consistent electrostatic field. These modifications enable the simulation tool to address several seminal questions concerning PTE. Several simulations have been performed and the influence of self-consistent modeling is addressed in this paper.

1 INTRODUCTION

A metric for measuring improvements in the painting process is Paint Transfer Efficiency (PTE) that measures how well paint is transferred from the bell applicator to the automotive body. Increases in PTE effect paint quality as well as costs since paint operations amount to a significant fraction of the total manufacturing cost of new automobiles. Improving the painting process will reduce manufacturing cost and improve appearance and durability which in turn directly influences customer satisfaction and warranty costs. A reduction in paint waste and emissions is also obtained by increasing PTE.

Quantifying PTE and determining the driving forces that improve the painting processes is difficult and requires extensive experimental testing. Many things affect PTE, ranging from applicator design to ambient atmospheric conditions. The painting process can be broken down into three distinct regions that ultimately determine its efficiency. The first, which we will call the near field region, involves the atomization process. Liquid paint is atomized and forms a distribution of particles within a short distance of the applicator. The bell design and rotation speed help to spread out the paint in the radial direction, while electrostatic repulsion further atomizes paint particle of like charge. This atomization process continues as the paint interacts with the shaping air and is ultimately directed toward the target.

The second is a transition region that couples the near-field atomization region and the far-field surface physics region at the target. The transition region is characterized by the interaction of the shaping air and atomized paint particles. Aerodynamic drag with the shaping air redirects the paint particles from a predominantly radial direction to an axial one towards the target. The third is the far-field region and involves particle impingement on the target. Surface physics dominates the amount of paint that is transferred to the target. One example of surface physics is for metallic paint where flake orientation determines the observed surface finish and

sheen.

While experimental testing can aid in determining PTE, the controlling parameters that maximize it are difficult to quantify. Experimental testing also produces emissions and paint waste as well as requiring engineering supervision. With demands to reduce automotive costs and emissions, new technologies are being developed to determine bell applicator and paintbooth designs. These techniques can augment experimental testing, reducing design space and shortening the design cycle. Computation Fluid Dynamics (CFD) is one technology that can aid bell applicator and paintbooth designs.

Even though significant improvements have been made in machine hardware and software architectures, modeling of PTE from first principles using CFD is still not feasible from a production environment. A CFD simulation engine would not only have to model the physics of atomization, but also the self-consistent interaction between the paint particles, shaping air and electrostatic field [1]. Since the paint has a density that is approximately 1000 time greater than that of air, the paint will modify the shaping air velocity distribution, requiring a self-consistent representation of their interaction. Electrostatic must also be modeled self-consistently whereby the presence of a charged particle affects globally all other charge particles. Not only does repulsion separate the particles but with a sufficient particle density the applied electrostatic potential is shielded. The CFD tool would also have to model the surface physics in order to accurately predict PTE.

Significant information, however, can be obtained by simply modeling the self-consistent interaction between the shaping air, paint particles, and electrostatic field. Using experimental data for the particle distribution, and assuming that all particles that hit the target contribute to PTE (i.e., neglecting surface tension effects, nucleation and movement on/off the target etc.), the effect of varying geometry and operating conditions on PTE by can be studied and quantified.

To this end, we have modified a commercially available CFD code to include the self-consistent interaction between the paint, shaping air and electrostatic field. These simulations were performed under varying operating conditions for different paint particle size distribution and potential drops.

We begin in section 2 of this paper with an overview of the numerical models used in this analysis. Section 3 describes the simulation domain and solid model used in this study, as well as the effects of bell operating conditions on PTE. We summarize our principal findings in section 4.

2 NUMERICAL METHODOLOGY

A commercially available CFD solver called FLOW-3D from Flow Science Inc. is used in this analysis. FLOW-3D represents a robust CFD solver capable of modeling the dynamic behavior of liquids and gases under a wide variety of physical processes such as heat condition, solidification, surface tension, and cavitation. The code has been constructed for the treatment of time-dependent problems in one, two and three dimensions whereby steady-state results are computed as the limit of a time transient.

FLOW-3D uses a fixed (Eulerian) grid of rectangular control elements. Unlike more traditional Navier-Stokes solvers, FLOW-3D uses a technique called the FAVOR (Fractional-Area-Volume-Obstacle-Representation) method to define general geometric regions within the rectangular grid. This method decouples the geometry and grid regions and eliminates the tedious task of generating body fitted or finite-element grids. The FAVOR method essentially uses partial control volumes to give the user the advantages of a body-fitted grid but retains the construction simplicity of an ordinary rectangular grid.

FLOW-3D is capable of modeling extremely complex fluid behaviors involving any number of independent free surfaces through the use of a Volume-of-Fluid (VOF) technique. The VOF method consists of three elements: a volume-of-fluid function for defining surfaces, a special advection method that maintains a sharp definition of the surfaces as they move and deform within the computational grid, and lastly the application of normal and tangential stress boundary conditions at the surfaces. The modeling of turbulent flows is accomplished through using any of the five different turbulence models provided by FLOW-3D: the Prandtl mixing length, one-equation, two-equation k-e and RNG models, and a large eddy simulation model. For the simulation presented in this paper, we chose a standard two-equation k-e turbulence model.

FLOW-3D has been modified to enable the modeling of discrete mass particles moving through a continuum. These modifications implicitly couple the particles and the continuum, so that they may exchange momentum in a conservative way. A momentum exchange term can be calculated and expressed as a force equal to a drag coefficient times the relative velocity between the two phases. Incorporating this force into the fluid momentum equation, and summing over the total number of particles, the particle drag on the fluid can be numerically modeled. The interaction becomes self-consistent and will satisfies a conservative relationship once a similar drag force is included in the particle's equation of motion.

The paint particle's equation of motion is not only influenced by drag with the shaping air, but by electrostatic forces. An electric potential difference is maintained between the paint applicator (~50-100 kV) and the target that is typically grounded (~0 kV). Paint particles that leave the bell assembly have an electric charge and are influenced by the presence of this external electric field. The modeling of the electric potential must be self-consistent since the particle charges contribute to the electric field. Consequently, the electric potential is time dependent and must be recomputed for each time step. FLOW-3D has been modified to include the determination of a self-consistent electric field by solving Poisson's equation. The charge density in each computational cell is determined and Poisson's equation is solved.

Through the inclusion of these two new functionalities in FLOW-3D, the influence of bell operating conditions as well as the dominance of shaping air and electrostatics on PTE are quantified in a self-consistent manner. This paper is a first attempt at numerically modeling a very difficult computational problem.

3 RESULTS

3.1 Solid Model and Simulation Parameters

Figure 1 illustrates the solid model used in the CFD simulation with the part dimensions listed in Table 1. The general construction of the bell (Figure 1A) involves a bell cup and housing, as well as a shaping air ring. The bell cup radius and axial length are 2.54 cm, with a shaping air ring of inner and outer radius of 1.15 and 2.54 cm, respectively. In order to simplify the simulation and reduce the required simulation time, the simulations presented in this paper assume a two-dimensional axisymmetric approximation. For some painting applications, such as side bells, this approximation is not valid due to the presence of not only gravity as well as a weak downdraft. Overhead bells, however, in which gravity is along the cylindrical axis satisfy this axisymmetric approximation.

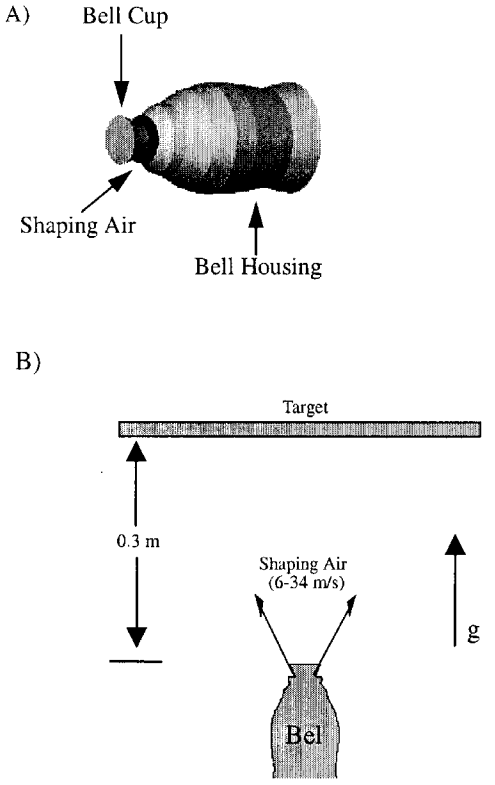

Figure 1: Bell simulation configuration

Figure 1b shows a typical applicator geometry located 0.3m (12 in) away a 0.3 m by 0.3m square target. A CAD representation of this geometry is used in the simulations. A source distribution for the shaping air is applied to a 3.86 cm^2 area of the shaping air ring as described in Table 1. The airflow is specified normal to the surface in the direction of the target (positive z direction). The source is applied to the entire cross-sectional area, unlike in actual test cases where high pressure forces the air through many small orifices. The shaping air ring mounts flush to the bell cup as well as to the bell housing which is 20 cm in length. The bell cup rotates at thousands of revolutions per minute while the paint is released on the inside of the bell cup. Through centripetal acceleration, the paint is radially accelerated and partially atomized.

TABLE 1: Tabulated Dimensions of CAD Parts used in the Numerical Simulations

CAD Part	Dimension [cm]
Bell Radius	2.54
Bell Length	2.54
Shaping Air Ring Inner Radius	1.15
Shaping Air Ring Outer Radius	2.54
Shaping Air Source: Inner Radius	1.90
Shaping Air Source: Outer Radius	2.20
Bell Housing	20
Target Wall distance	30
Target Wall Length	30

Bell operating conditions vary extensively depending on the applicator design and paint type. In order to quantify the relative importance of self-consistent effects and operating conditions on PTE, nominal values have been chosen for the numerical simulations and are presented in Table 2.

TABLE 2: Modeled Operating Conditions

Shaping air density	1.205 kg/m3		
Shaping air flow rate	150 l/min	300 l/min	
Paint density	1205 kg/m3		
Paint flow rate	160 ml/min	240 ml/min	
Bell speed	10 krpm	30 krpm	
Electric Potential	60 kV	90kV	120kV

The paint density has been chosen to be 1000 times that of air while the electric potential is applied only the bell cup with all the other surfaces maintained at ground.

Figure 2 shows the 2D axisymmetric configuration for the bell applicator simulations presented in this paper. The bell housing, bell cup, and shaping air ring are positioned in the lower left hand side of the r-z coordinate as shown in Figure 2a. The top of the bell cup is located at z=0 and extends in the radial direction to 2.5 cm. Gravity is in the positive z-direction resulting in particles accelerating toward the target which is positioned 0.3 m from the bell cup. The simulation domain extends from –20 cm to 40 cm in the z-direction and 0 cm to 40 cm in the radial direction. All units and dimensions if otherwise specified are in CGS units.

The rectangular volume mesh for FLOW-3D can be found in Figure 2b. Even with the FAVOR method, the positioning of a concentrated mesh region is required in order to accurately model the expansion of the shaping air. Figure 2b shows a region of higher resolution around the shaping air ring and directed toward the target. Simulations have been run using this meshing strategy and have shown good agreement with experimental data.

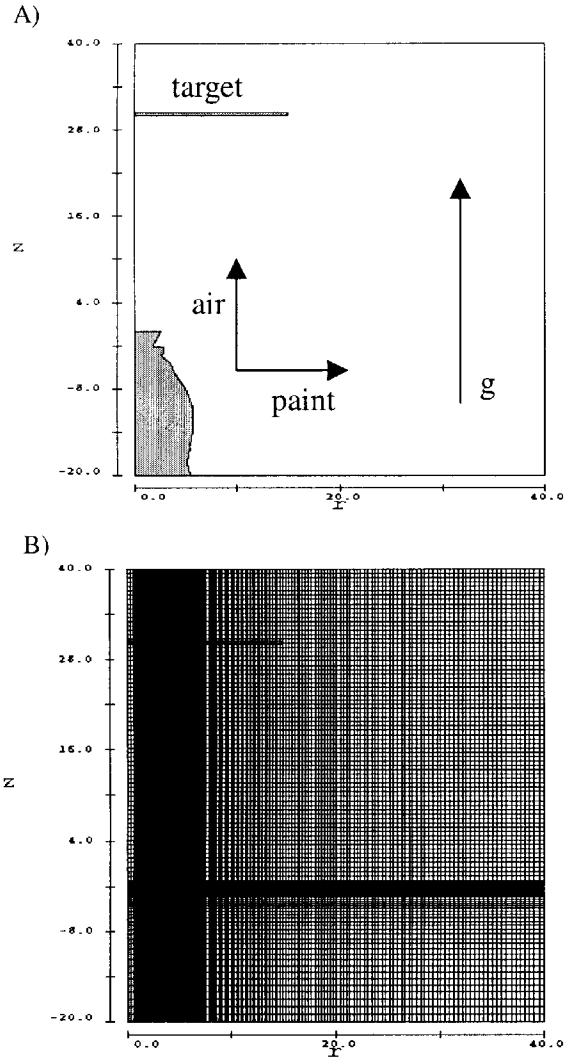

Figure 2: Simulation configurations (A) and mesh (B).

The simulation assumes pressure boundary conditions on the top wall at z = 40 cm and side wall at r = 40. Symmetry is assumed at r = 0 cm while a hard wall boundary condition is applied at z = -20 cm.

Each simulation presented in this paper used the same volume mesh with 160 and 120 cells in the z and r direction, respectively. The simulations required approximately 24 CPU hrs on an SGI Octane to reach steady-state which corresponds to 0.4 seconds in the simulation. Due to an efficient implementation of the self-consistent momentum coupling and electrostatics, no appreciable time increase was observed by invoking these interactions.

3.2 Shaping Air

The shaping air is modeled by specifying a mass flow rate on a ring which has an effective area of 3.86 cm^2 as described in Table 1. Using an air density of 1.205 kg/m^3, a mass flow rate of 0.003 kg/s and 0.006 kg/s is prescribed for an air flow rate of 150 l/min and 300 l/min, respectively.

Figure 3 shows the velocity magnitude in z-direction for the shaping air at 150 l/min. The air expands outward and interacts with the rotating bell cup in Figure 3A. The shaping air expands above the bell cup (positive z-direction) and induces, through shear flow, a recirculation near the bell cup center as shown in Figure 3B. Shear flow stresses also induce a predominant rolling vortex on the opposite side of the flow structure (r > 2.5cm) as it travels toward the target. Steady-state flow results can be obtained by running the simulation longer in time. Figure 3C shows steady-state behavior in the flow; however, due to the inherent transient nature of the flow dynamics, oscillations in the flow structure at the target can be seen in Figure 3D. Qualitatively, the structure is the same even though small variations in the velocity magnitude and spatial structure are observable.

The shaping airflow becomes more diffuse once the flow has interacted with the rotating bell cup. Typical bell applicator designs introduce a slight blockage of the shaping air by the bell cup. The amount of blockage depends on the bell design; however, the blockage introduces a small azimuthal velocity component to the shaping air. This azimuthal velocity component helps to entrain paint particles and direct them to the target. Figure 4 shows the azimuthal velocity for the same conditions and times as that presented in Figure 3. The azimuthal velocity is approximately 5 m/s and is about a sixth of the velocity magnitude in the z-direction.

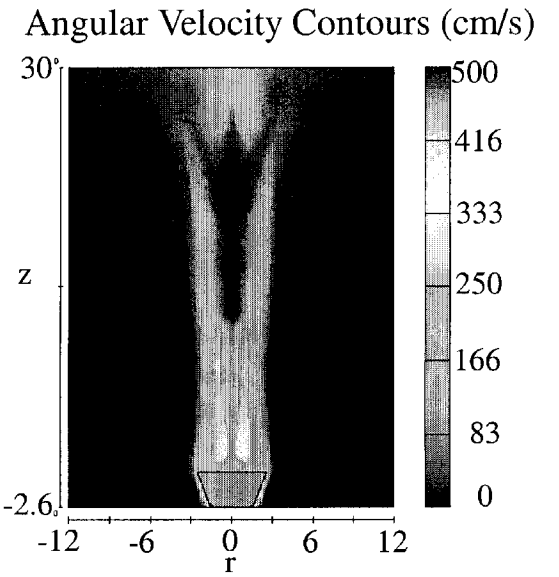

Figure 4: Azimuthal velocity contours.

Various rectangular volume meshes and turbulence models have been used in order to determine the optimal simulation configuration. The simulations in Figures 3 and 4 used a two-equation k-e model and the volume mesh presented in Figure 2B. The resulting simulations were compared to experimental shaping air measurements and excellent agreement was obtained.

3.3 Particle Injection

Since the atomization process is not modeled from first principles, a particle size distribution must be assumed. Figure 5 shows a representative particle distribution that is

characteristic of many applicator and spray technologies. For most atomization process, the distribution of particle sizes is Gaussian in nature and is centered about one preferential particle size as demonstrated in Figure 5.

Particle injection requires information about the flow rate and density of the phase that is being modeled by particle injection. These two parameters, and knowledge of the effective area over which the flow is injected, enables the determination of the injection rate as well as the velocity which conserve mass and momentum. Particle injection can be modeled using a PDF (probability-distribution-function), and through the selection of random number, an injected particle is assigned a particle size in accordance with a distribution similar to that in Figure 5.

For our purposes, we used a histogram representation of the particle distribution and assigned a relative weighting between size partition. The maximum of the distribution corresponds to P3 (partition 3) and all other contributions to the particle distribution function are normalized to P3. It is assumed that P2=P4=.75P3 and P1=P5=0.5P3. Using the operating conditions for the bell applicator (Table 2), a simple relationship can be solved which determines the particle generation rate (number of particles per second).

The particle velocity is assumed to be radial and equal to the angular velocity of the rotating bell cup ($V=2\pi Nr$ where r is the bell cup radius and N is the rotation speed of the bell). The paint particles are emitted z=0 and at a radial distance of approximately 2.5 cm, which corresponds to the edge of the bell cup. Table 3 shows the particle generation rate and relative contributions for P1 to P5.

Table 3: Particle Generation Rate as a Function of Paint Flow Rate. Generation rate corresponds to the number of particle per second, while the flow rate is in ml/min.

Flow Rate	P1	P2	P3	P4	P5
160	350	528	698	528	350
240	524	785	1047	785	524

The injected particles for P1 through P5 are generated randomly in each partition based upon location, size, and generation rate.

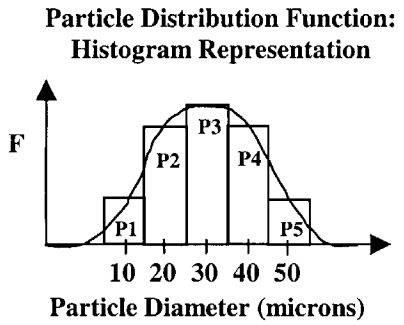

Figure 5: Particle distribution function.

Using the distribution characterized by Table 3 and Figure 5, particle trajectories are shown in Figure 6. The operating conditions are *(bell speed, shaping air flow rate, paint flow rate, particle size) = (30krpm, 150 l/min, 240 ml/min, all).* Each particle is created with the local tangential velocity of the rotating bell cup. Consequently, for a bell cup rotating at 30 krpm and with a radius of 2.5 cm, particles are given a radial velocity of approximately 78m/s. Figure 6A shows a radial spatial separation between particles of varying size with the largest diameter particles traveling farthest from the bell applicator.

All particles are interacting with the shaping air as well as the ambient air through drag forces. These drag forces dissipate the particle's kinetic energy and slow the particles. Larger particles, having more mass and therefore kinetic energy, require more time to dissipate their energy thereby creating the spatial separation as a function of particle size as shown in Figure 6A. The region of influence for the shaping air, as modeled in this paper, is localized to approximately 1 cm on either side of the bell cup (Figure 3). As particles are created and traverse this radial extent, each particle spends 0.13 milliseconds in the shaping air. Subsequently, only small particles are significantly affected by the shaping air and are immediately entrained into the shaping air.

Figure 6B shows that 20 micron size or smaller particles are entrained into the shaping air and have propagated downstream to the target by 0.123 seconds. Larger particles, however, once they have traversed the shaping air are only influenced by gravity. As the particles approach the target, complicated flow fields due to the interaction of the shaping air with the target entrain particles. Particles with diameters less 40 microns are entrained, larger particles are deflected away from the target. Figures 6C and 6D show particle trajectories as well as velocity contours of the shaping air. The transient nature of how the shaping air interacts with the target will affect particle transfer to the target. Figures 3C and 3D show a non-steady interaction of the shaping air with the target, and as observed in Figures 6C and 6D, affects paint transfer. Typical bell applicators as well as the target move during the paint process and affect paint deposition on the target. Future work will focus on including these affects.

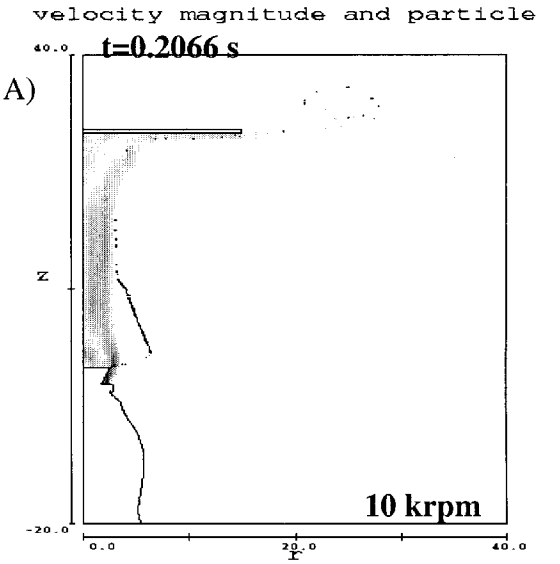

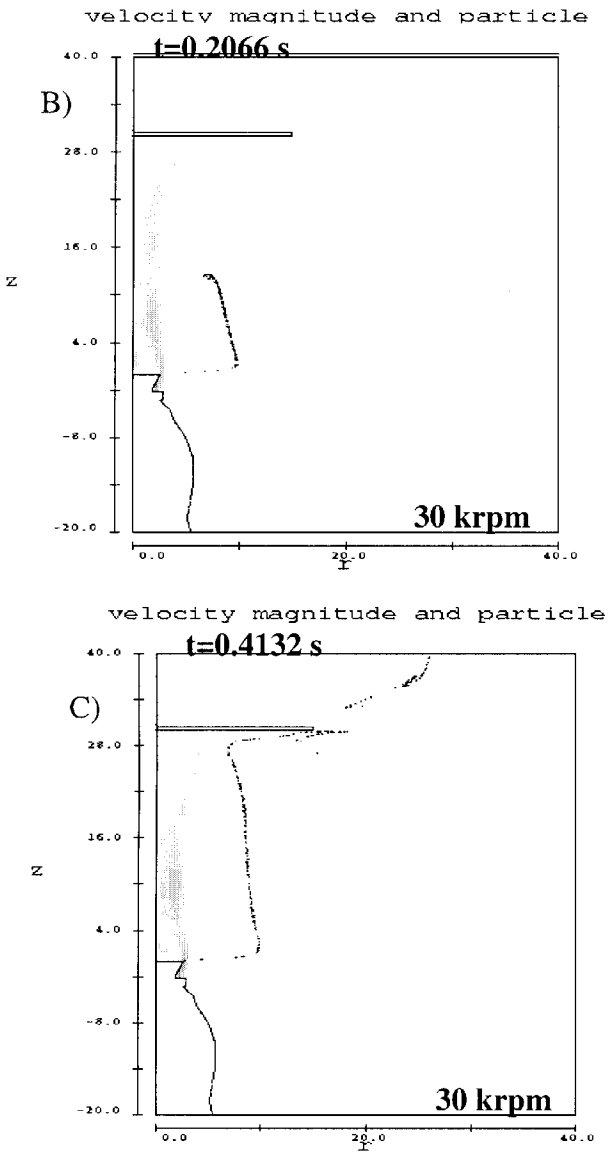

Figure 7: Particle trajectory as a function of bell speed.

Operating conditions such as bell speed, shaping air flow rate, and paint flow rate affect PTE. Figure 7 shows the influence of bell speed on 30 micron size particles. The simulations presented in Figure 7 vary the bell speed from 10 krpm to 30 krpm, while all other conditions are held constant *(varied, 150 l/min, 240 ml/min, 30 microns).* The particle's radial velocities are 26 m/s and 78 m/s for the bell speeds of 10 krpm and 30 krpm, respectively. Steady-state results were achieved in 0.2 sec for the 10 krpm simulation presented in Figure 7A. The 30 micron paint particles travel through the shaping air, are influenced by gravity and start moving toward the target. Interestingly, entrainment of the paint particles occurs at z = 10 cm. Ambient air, through shear flow affects, is not only directed downstream to the target but radially inward toward the shaping air.

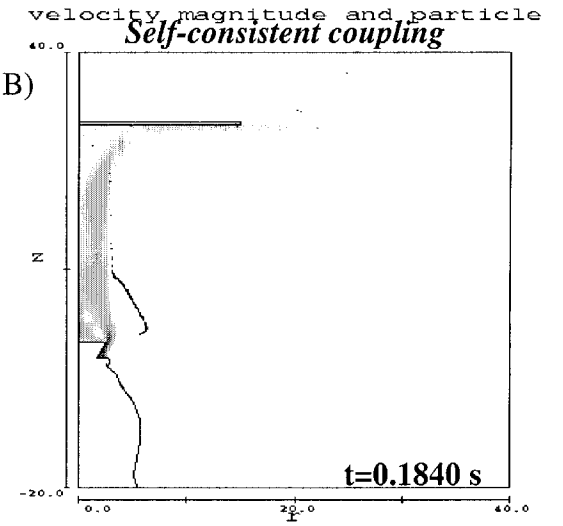

Figure 8: Particle trajectory comparison between a non-conservative and conservative model describing the interactions between the air and paint particles.

This same phenomenon can be seen in Figures 7B and 7C, however, the particles are not entrained. At 30 krpm, the particle's maximum radial extent is 10 cm which is larger than that obtained for the 10 krpm simulation. The particle trajectories in Figure 7A and 7B are taken at the same time, t=0.2 sec. Paint particles in Figure 7B have only propagated 12 cm in the z-direction while Figure 7A shows the particles impinging the target. Without entrainment, the particles are only under the influence of gravity. Consequently, steady-state results presented in Figure 7C were obtained in 0.4 seconds, which twice the time is required for the 10 krpm simulation.

Decreasing the shaping airflow rate results in a decrease in the airflow velocity. This inevitably reduces not only the level of entrainment but reduces the effects of drag since the drag term is proportional to the relative velocity difference between the phases. Paint flow variation must be analyzed with the inclusion of self-consistent effects such as electrostatics and momentum coupling and is the subject of the next two sections.

3.3 Self-consistent Drag Effects

Figure 6 shows the particle trajectory of paint particles that are experiencing a non-conservative drag force [2]. Under these circumstances, the continuum variables (density, velocity etc.) are used to influence the particle's motion however there is no corresponding relationship where the particles motion affects the continuum. There are many circumstances where this approximation is valid; however, as the particle density increases relative to the continuum density, the discrete mass particles can affect the continuum momentum to a greater extent.

Flow-3D's continuum momentum equation has been modified to include a source term responsible for the momentum coupling between the phases. This term enables a conservative modeling of the interaction between the shaping air, ambient air, and paint particles. Figure 8 shows the influence of self-consistent momentum coupling. In this case, Figure 8A (non conservative) and Figure 8B (conservative) show identical shaping-air contours and particle trajectories. Consequently, the presence of discrete mass particles has no appreciable effect on the continuum state.

Several factors contribute to minimize the influence of the paint on its surrounding. The first of which is the flow rate that is orders of magnitude lower than the shaping-air flow rate. Even though the paint density is much larger, the low flow rate minimizes the coupling between both species. The atomization process is one region where strong momentum coupling between the liquid paint and shaping air exists. This coupling as well as electrostatics is critical for breaking up the paint ligaments into discrete atomized particles. Bell cup surface geometry also play a role in the atomization process.

A second factor comes from the limited area of influence of the shaping air. Above the bell cup, dispersion of the shaping air accounts for the broadening of the radial extent of the source. The shaping air near the bell cup, however, has a 1 cm radial extent through which the paint and shaping air interact. Modification of the bell applicator design may show more of an effect due to momentum coupling; however, for the geometry simulated in this paper, the shaping-air and paint coupling near the bell cup is not significant, at least from the perspective of modifying the shaping air flow field. More studies are needed to determine in what regime this coupling is important. By adding downdraft, movement of the geometry such as the bell applicator or target, and resolving the flow in 3D, stronger momentum coupling may be observed.

3.4 Self-consistent Electrostatics

Electrostatic is used routinely in painting applications as a way to increase atomization and help direct the flow to the target. Another motivation for using electrostatics is to increase PTE locally near the target. In this region, electrostatic forces can dominate over inertial forces from the shaping air and its interaction with the target. The target is typically maintained at ground, resulting in a net force of attraction between the paint particles and target.

A test particle approach can be used to investigate the influence of an electric potential on the trajectories of paint particles. One difficulty with this approach is that the presence of charged particles will modify locally the electric field. For a sufficient number of particles, the electric field can be significantly modified requiring a self-consistent solution to determine the electric potential. By summing the electric charge density of the particles, Poisson's equation can be solved and a self-consistent electric potential determined. Once a potential is know, each particle will experience a force due to the presence of this field.

Figure 9 shows particle trajectory under the influence of electrostatics. The operating conditions for the simulations are *(30 krpm, 150 l/min, 240 ml/min, 30 microns)* with the only difference being the magnitude of the electric potential. The charge-to-mass ratio used in the simulation was taken from experimental results [private communications, Chigier, Carnegie Mellon University] and assumed to be 10 mC/kg (the experimental results for 30 micron size particles at 40 kV is ~ 0.01 Coulombs/kg). Given the paint density and particle diameter, each particle is given a charge commensurate with the above charge-to-mass ratio. Figures 9A and 9B assume a zero electric potential, while Figures 9C and 9D use an electric potential of 90 kV.

Figures 9A and 9C are taken at t = 0.2 seconds into the simulation and show particles colorized by their z-component velocity. Both figures have the same initial structure for $z < 3.0$; however, electrostatic repulsion, as shown in Figure 9C, not only weakly accelerates the particles toward the target but causes the front edge of the particle beam to expand. This process continues and is shown in Figures 9B and 9D at 0.3 seconds. Clearly, electrostatic repulsion is significantly influencing the particle's motion at 90 kV. Under these circumstances, the particle tracks on the target would be more diffuse at 90 kV (Figure 9D) than at 0 kV (Figure 9B).

4 CONCLUSION

Using a commercially available CFD package, we were able to investigate the influence of particle size, operating condition, and the impact of self-consistent momentum coupling and electrostatics on paint particle dynamics. A CFD simulation called FLOW-3D was modified to include momentum coupling between a continuum and discrete mass particles. A momentum source term is included in the continuum momentum equation and models momentum variation caused by discrete mass particles. By solving the continuum equations, coupled with a simple drag relationship for the discrete particles, FLOW-3D is capable of modeling the momentum exchange between the shaping-air, ambient air, and paint particles in a self-consistent manner.

FLOW-3D was also modified to include self-consistent electrostatic fields. Many paint applications use electrostatics to improve atomization and paint transfer efficiency. Charged particles not only experience a force due to the electric potential but ultimately modify the electric potential due to their presence. Consequently, a self-consistent treatment is required in order to accurately determine the electric potential. Poisson's equation is solved every time step, producing a new

electric field which is used to move the particles.

The painting process is inherently transient and involves moving geometry as well as transient flows. The simulations presented in this paper assume that the geometry is stationary; however, moving geometry is possible in the framework we have adopted. The atomization process is difficult to model from first principles so we assume an atomized particle distribution that is consistent with experimental findings.

The simulation accurately modeled the shaping air production and its interaction with a rotating bell cup and show good qualitative trends as compared to data [3]. The shaping air showed a transient nature near the bell cup, as well as at the target. A moving target or bell applicator would likewise introduce more transients into the already unstable flow. The shaping air initially has only a component in the z-direction (Figure 3); however, by interacting with the rotating bell cup, a tangential or azimuthal velocity component is introduced (Figure 4) which aids in particle entrainment. The shaping air interacts with the ambient air and introduces, through shear flow forces, a recirculation that entrains particles. Consequently, particles experience an inwardly directed radial force, focusing the particle and directing them toward the target as depicted in Figures 6, 7, 8 and 9.

Smaller diameter particles are affected by the shaping air and are entrained into the shaping airflow immediately. Larger particles, however, travel through the shaping air and eventually come to rest by dissipating their kinetic energy to the ambient air. The particle density is sufficiently high to warrant a conservative momentum coupling approach; however, the number density of particle is very low resulting in a minimal momentum change to the continuum from the discrete particles. Consequently, a self-consistent momentum coupling of the paint and shaping air introduced no observable affect (Figure 8).

Self-consistent electrostatics, however, showed a significant repulsion between the charged particles (Figure 9). The paint particle not only formed a broad beam of particles, moving toward the target, but experience a slight acceleration. In both cases the particles will deposit on the target; however, electrostatic will introduce a larger footprint on the target.

We have a simulation tool and methodology that is capable of modeling many of the nonlinear physical properties associated with paint applicators. With the addition of self-consistent momentum coupling and electrostatics, we are in a position to understand the inherent complexities associated with PTE. Future work will center on developing a Design Of Experiments (DOE) using the simulation tool to optimize bell performance and paint transfer efficiency across operating conditions as well as bell design.

ACKNOWLEDGMENTS

The authors are grateful to C. Wu and I. Salmeen who have supported this effort and to T. Loch who have provided insightful discussions on paint technology and applications.

REFERENCES

1. Miller, R., G. Strumolo, V. Babu, J. Braslaw, and M. Mehta, " Transient CFD Simulations of a Bell Sprayer," Proceedings of the International Body Engineering Conference & Exposition, SAE Paper No. 982291, 1998.
2. Schlichting, H., Boundary Layer Theory, McGraw-Hill, New York, 1955.
3. Skender, M. M., and J. Braslaw, "Optimizing Basecoat Application with Rotary Bell Atomizers," Proceeding of the 3rd Annual ESD Advance Coatings Conference, ACT, p 289, published by ESD, The Engineering Society, Ann Arbor, MI. ,1993.

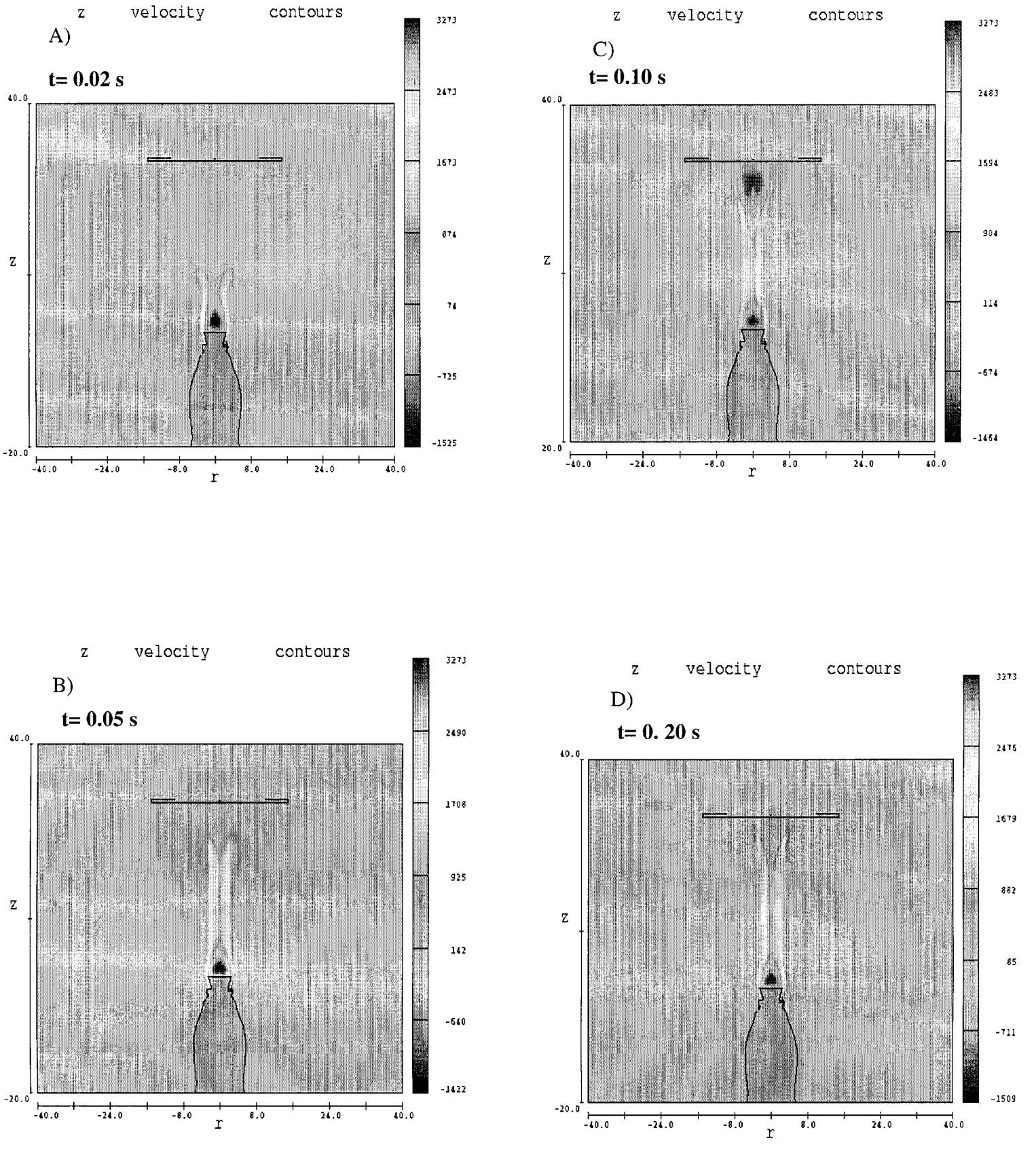

Figure 3: Z-V

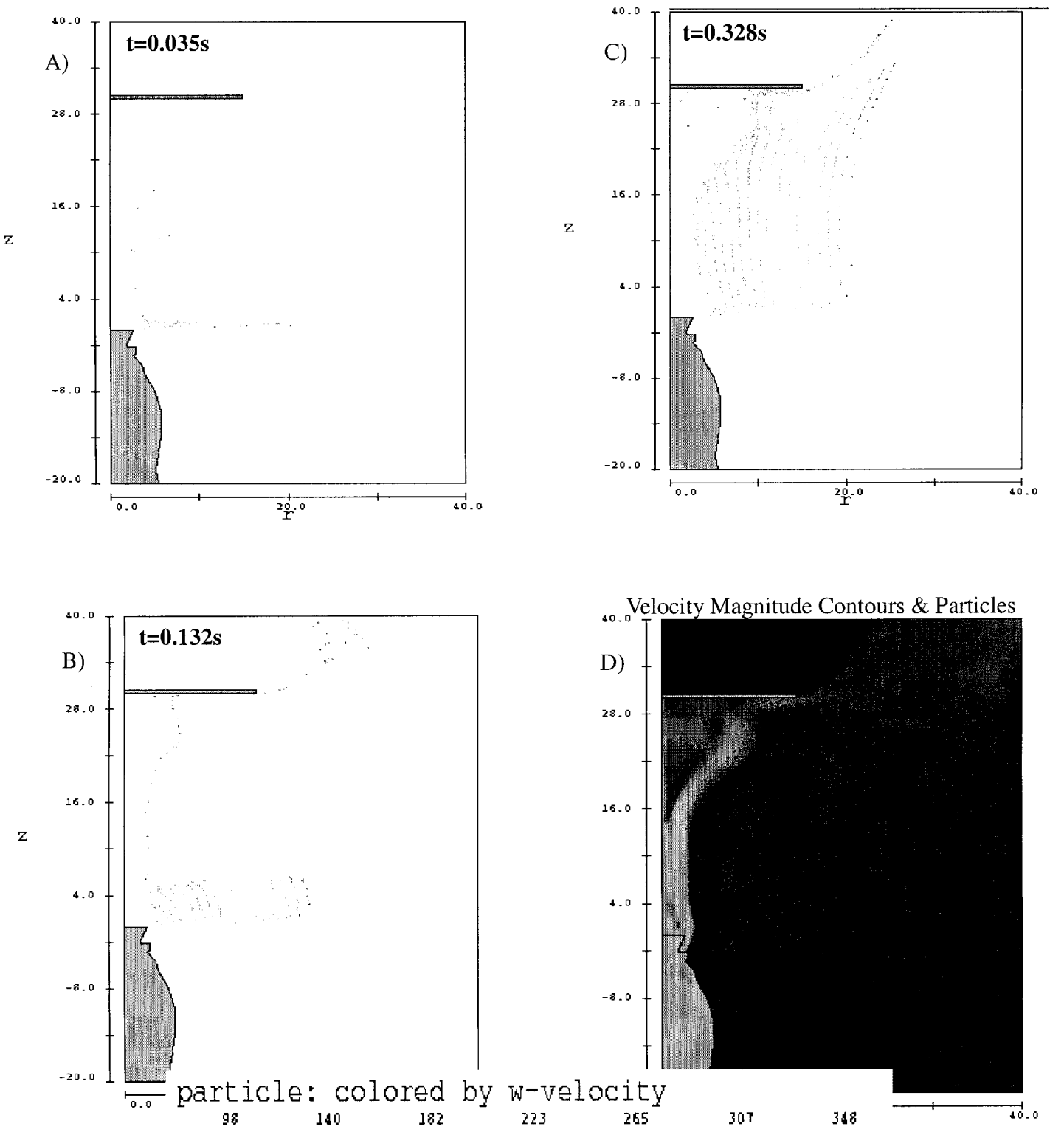

Figure 6: Paint pat[illegible] attachment hours as a function of particle size and time.

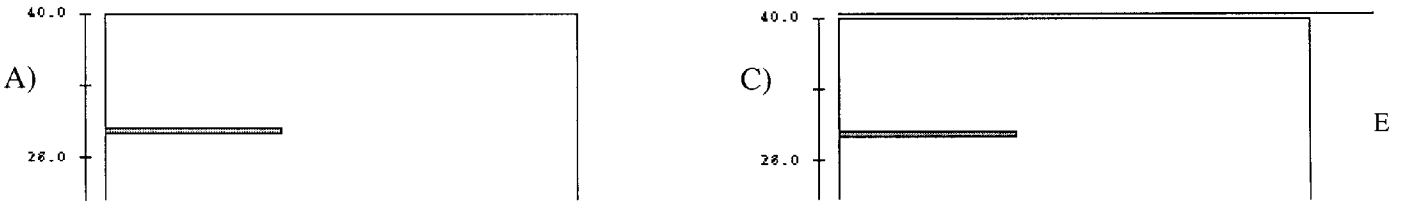

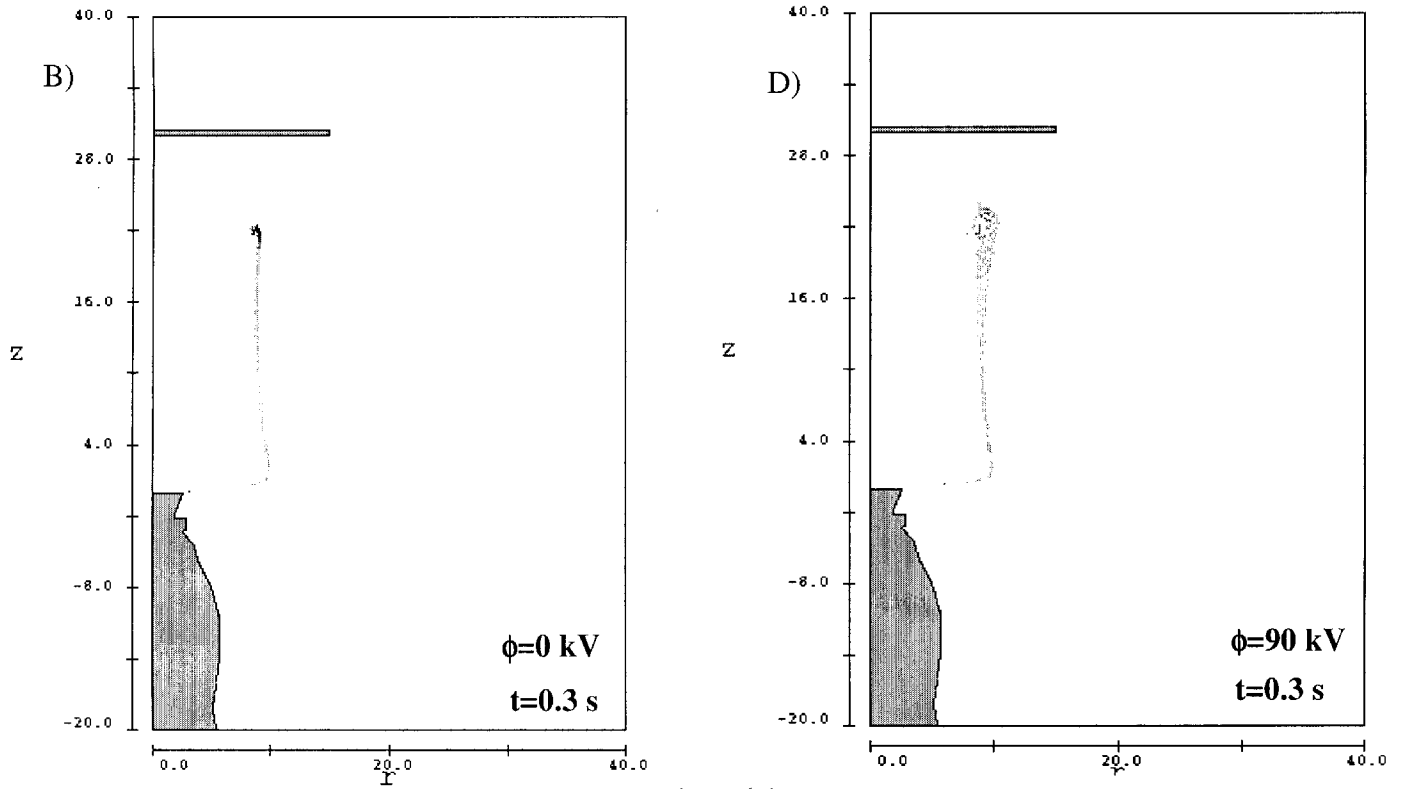

Figure 9: Paint particle trajectory plots as a function of particle size and time